Mon. Not. R. Astron. Soc. **000**, 000–000 (2000)

Reconstructing the History of Star Formation in Rich Cluster Cores

Tadayuki Kodama[1,2] and Richard G. Bower[1]
[1] *Department of Physics, University of Durham, South Road, Durham DH1 3LE, UK*
[2] *Department of Astronomy, University of Tokyo, Hongo, Bunkyo-ku, Tokyo 113-0033, Japan*

Submitted to Monthly Notices of the Royal Astronomical Society since 9th Feb 2000.

ABSTRACT

Our study begins by revisiting the *photometric* Butcher-Oemler effect using data from the 7 CNOC clusters at $0.23<z<0.43$. We construct the foreground/background corrected colour-magnitude diagrams for these clusters. Our analysis shows that the CNOC clusters reproduce the trend of blue fraction with redshift as shown for a larger sample by Butcher & Oemler. We use these data to investigate the history of star formation in clusters by connecting the snapshots at different redshifts. We address two key issues: Firstly, we ask whether the simple fading and passive evolution of the blue galaxies is consistent with the properties of galaxies in nearby clusters, such as the Coma cluster. We find that reddening of star forming field galaxies on entry into the cluster environment, can successfully reconstruct colours and magnitudes of galaxies in the local cluster, and hence there is no requirement for widespread disruption of these galaxies: to within the limits of this distant cluster data. Secondly, we address the nature of the Butcher-Oemler effect itself: the increasing fraction of blue galaxies with redshift. We compare the distribution of galaxies in the colour-magnitude diagrams and hence infer the evolution of the rate at which galaxies have arrived in the cluster. Models in which star formation is abruptly truncated as galaxies are accreted by the cluster have difficulty in reproducing the observed colour distribution. In contrast, if star formation declines on a 1 Gyr timescale after accretion, the infall history we infer is consistent from cluster to cluster and matches well the distribution expected in simple theoretical models. The Butcher-Oemler effect is thus driven both by the declining star formation rates of field galaxies and by a decline in the rate at which fresh galaxies are accreted by the cluster. Our study naturally leads to a comparison of the global star formation histories of galaxies in clusters and the field. We show that the star formation rate per galaxy mass for the galaxies in the cluster cores is significantly smaller than that of the field environment below $z<1$ due to the truncation of star formation.

Key words: galaxies: clusters – galaxies: formation – galaxies: evolution – galaxies: stellar content

1 INTRODUCTION

It is 20 years since Butcher & Oemler (1978; 1984, hereafter BO84) first reported their startling results on the blue galaxy fractions of distant clusters. This and subsequent photometric work suggested that the cores of distant clusters at redshift $z>0.2$ contained large numbers of blue galaxies (Couch & Newell 1984; Lubin et al. 1996; Rakos & Schombert 1995), in stark contrast to the homogeneous red populations of local galaxy clusters (eg., Bower, Lucey & Ellis 1992; Terlevich, Bower & Caldwell 2000). There has been a suggestion of apparent contradiction between the narrow colour-magnitude (CM) relation of evolved galaxies in local clusters (which indicates a long period of passive evolution) and the intermediate redshift blue galaxies (which indicate considerable relatively recent star formation activity). In Bower, Kodama & Terlevich (1998, BKT98) and Balogh et al. (2000), they have begun the process of modelling the combined dynamical and photometric evolution of clusters in order to reconstruct the galaxies' formation histories.

The original definition of the BO galaxies involved only the photometric properties of galaxies. We will refer to this aspect as the 'photometric Butcher-Oemler effect'. Dressler & Gunn (1992) and Couch & Sharples (1987) un-

dertook spectroscopy initially with the motivation of confirming spectroscopically that the blue galaxies were cluster members. They discovered that many of the blue cluster galaxies, and some red ones, had spectra of a type that are rare in local galaxy samples. These galaxies (E+A, PSG, A+K) have anomalously strong Balmer lines indicating an excess of A-stars superimposed on an K-star type spectrum. The galaxies are produced when star formation is abruptly truncated (Couch & Sharples 1987). The strongest lined examples require a burst of star formation just before the truncation (eg., Barger et al. 1996; Poggianti & Barbaro 1996; Poggianti et al. 1999; Couch et al. 1998). We refer to the increase in the incidence of such spectra as the 'spectroscopic Butcher-Oemler effect'

With the advent of HST, it has become possible to study the morphologies of galaxies in the distant clusters (Smail et al. 1997; Dressler et al. 1994; 1997; Couch et al. 1994; 1998). They found that the morphological mix in these clusters also evolved with redshift creating a third variant of the Butcher-Oemler effect, which we will refer to as the 'morphological BO effect'. Several attempts have been made to link between photometric/spectroscopic features and the morphology. Dressler et al. (1994) and Couch et al. (1994) showed that most of the blue BO galaxies are actually normal spirals with the rest being interacting galaxies or mergers. Poggianti et al. (1999) compared the spectroscopic and the morphological effects, suggesting that the time scale of the morphological transition is longer than the A-type star evolution since the post star burst galaxies (K+A/A+K) are observed as normal spirals rather than S0 galaxies.

In this paper, we aim to clearly separate these three different (but related) evolutionary trends. We will focus on the *photometric* effect, returning to the questions raised by Butcher & Oemler's original papers. Our aim is to look at the CM diagrams of the distant clusters in more detail, examining how the blue fraction varies with the magnitude of the galaxies and with radius in the cluster. The variation with magnitude is of interest given Cowie's claim of cosmic 'down-sizing': the progression of star formation into smaller and smaller units as the universe ages (Cowie et al. 1996). We wish to see whether this process is mirrored in the cluster galaxies as well as the field. Because of the existence of a density morphology relation (Dressler et al. 1997), we should expect radial gradients in the colours and blue fraction. At very large radii, the blue fraction should reach the field value. In order that we can make a meaningful comparison between the local and distant clusters, it is important that this effect can be quantified.

Our goals in this paper in this paper are two-fold. Initially, we will make an accurate comparison of the distant and local clusters. In particular, we will test whether the galaxies in the distant clusters simply fade and redden after their star formation is truncated or whether an additional mechanism such as tidal stripping or harassment (Abadi et al. 1999; Moore et al. 1996) is required to explain how the distant clusters evolve into clusters like those at the present-day. We then go on to explore the distribution of galaxies in the colour-magnitude plane, and to address the difference between clusters at different redshifts. The distribution of galaxies can be used to compare the rate of infall when the cluster is observed, with that at earlier times. We will show that a consistent picture emerges in which the declining rate at which fresh galaxies are accreted by the cluster, combined with the declining activity of field galaxies, accounts for the evolution of the Butcher-Oemler blue-galaxy fraction.

The layout of the paper is as follows. In § 2, we present the sources of data used to compose the distant and local cluster CM diagrams, and outline how we correct for background and foreground galaxies. In § 3, we calculate the blue galaxy fraction from the field corrected CM diagrams and discuss its dependence on magnitude and the distance from cluster centre. In § 4, we apply our stellar population models to calculate the reddening and fading of the distant cluster CM diagrams and compare with a local cluster Coma. In § 5, we investigate the colour distribution of galaxies in more detail, examining how the galaxy infall rate must evolve in time. Our conclusions are reiterated in § 6.

We use H_0=50 km s^{-1} Mpc^{-1} and q_0=0.1 throughout this paper, which are the same parameters adopted in the original BO work. The age of the universe is 16.5 Gyr for this parameter set.

2 PHOTOMETRIC DATA FOR CLUSTERS OF GALAXIES

2.1 Distant Clusters

We use 7 distant clusters from the CNOC survey (Yee et al. 1996) at redshifts between 0.23 and 0.43 as summarised in Table 1. The CNOC clusters are selected using the EMSS catalogue of X-ray bright clusters (Gioia & Luppino, 1994). Our sample clusters are all X-ray bright with $L_X = 4-28\times 10^{44}$ erg s^{-1} (0.2-3.5 keV), which is comparable to our local sample Coma whose $L_X = 8.1\times10^{44}$ erg s^{-1} (Yee et al. 1996; Ebeling et al. 1996; see Table 1 of this paper). The advantage of using the CNOC sample is that they obtained ∼100-300 redshifts per cluster and also the field of view both for the imaging and the spectroscopy is relatively large. This helps in determining cluster membership accurately. Furthermore, the wide field enable us to investigate systematic change of stellar populations as a function of distance from the cluster centre (eg., Abraham et al. 1996).

The photometric data use the g and r bands in Gunn's system. The effective wavelengths are roughly 4900 Å and 6500 Å and the $g-r$ colour brackets the 4000 Å break in the rest frame for our sample clusters. Therefore $g-r$ colour has good sensitivity to the stellar populations in the cluster galaxies. Also it is relatively easy to transform the observed colours into the rest frame $U-V$ colour as we will do later. They used a fixed diameter aperture of 6.4, which is 31-46 kpc for z=0.23-0.43. The completeness limit is about r=23.5 magnitude. We use the only galaxies brighter than this limit in this paper. Even so, the photometric data has relatively poor accuracy compared to the data available for local clusters. The typical photometric error reaches to ∼0.2 magnitude at r∼23 mag.

2.2 Matching the Cluster Radius

One of the key ingredients required to make the accurate comparison of cluster galaxies between local and distant clusters is to match the area over which the comparison is made. We use R_{30}, the radius from the cluster centre which

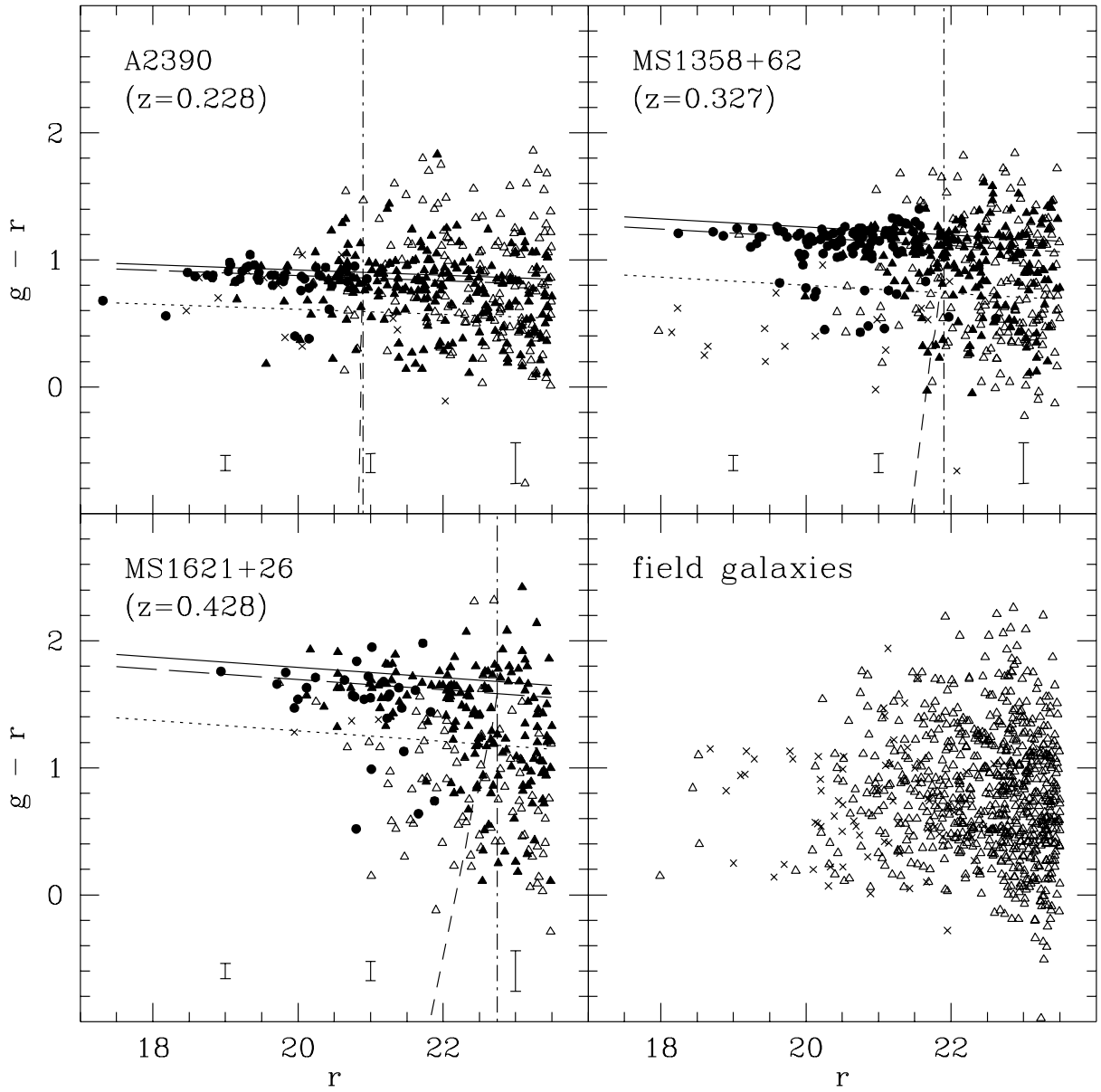

Figure 1. Colour-magnitude diagram for the three clusters, A 2390 (top left), MS 1358+62 (top right), and MS 1621+26 (bottom left), and for the field taken from the edge of the four cluster fields (bottom right; see text). *Filled circles*: Spectroscopically confirmed members. *Crosses*: Spectroscopically confirmed non-members. *Filled triangles*: Statistically plausible members. *Open triangles*: Statistically subtracted non-members. *Horizontal long dashed line*: The CM red sequence assuming the pure metallicity sequence. *Solid line*: The red envelope (see text for definition). *Dotted line* Colour limit of the blue galaxies corresponding to the BO's limit of $\Delta(B-V)=-0.2$ from the red sequence. *Vertical dashed line*: Magnitude cut, $r_{\rm cut}$, corresponding to $M_V=-20$ in the rest frame as in BO. *Error bars*: Typical photometric errors (one sigma).

Table 1. Summary of our cluster samples

cluster	z	L_X ‡ 10^{44} erg/s	δRA $\times$ δDEC arcmin^2	$t_{\rm LB}$ Gyr	R_{30} arcmin	$r_{\rm cut}$ mag	CM slope	CM zero-p	$\Delta(g-r)$	f_B
A2390	0.228	23.8	46 × 7	3.59	2.77	20.90	−0.020	0.89	−0.27	0.106 ± 0.034
MS1008−12	0.306	4.5	9.0 × 7.9	4.52	2.82†	21.71	−0.029	1.20	−0.37	0.161 ± 0.035
MS1224+20	0.320	4.6	9.0 × 7.1	4.67	2.74†	21.84	−0.031	1.12	−0.38	0.177 ± 0.054
MS1358+62	0.327	10.6	9.0 × 23.3	4.75	3.58	21.90	−0.032	1.16	−0.39	0.106 ± 0.027
MS1512+36	0.371	4.8	27.3 × 8.0	5.21	3.26	22.27	−0.037	1.18	−0.42	0.378 ± 0.070
MS0302+17	0.425	5.0	9.0 × 7.9	5.73	2.31†	22.72	−0.041	1.46	−0.42	0.206 ± 0.065
MS1621+26	0.428	4.5	9.0 × 23.3	5.75	2.18	22.75	−0.041	1.64	−0.42	0.160 ± 0.036
Coma	0.024	8.1	63 × 53	0.46	22.0	—	—	—	—	0.056 ± 0.028

Note – † R_{30} is assumed to 1 Mpc for these clusters due to the relatively small spatial coverage.
‡ X-ray luminosity in a band, 0.3-3.5keV.

contains 30 per cent of the whole cluster populations, following BO84.

R_{30} is determined using the galaxy distribution from the cluster centre after subtracting the average number density of field galaxies taken from the edge of the cluster field (see below). We take into account the rectangular shape of the observed fields. We measured R_{30} for four clusters, namely, A2390, MS1358+62, MS1512+36, and MS1621+26, and are given in Table 1. Our estimates are in very good match with those of van der Marel et al. (1999) except for MS1512+36. As we will discuss later, MS1512+36 is likely to be contaminated by a foreground group or cluster, making R_{30} estimate difficult. For the remaining three clusters, it is impossible to obtain R_{30} because of their small spatial coverage. Therefore we had to assume R_{30} to be 1 Mpc (H_0=50) in physical scale for these clusters, which is the typical radius that we measured for the other clusters. This may be in error by ∼30 per cent due to fluctuation of the background field galaxy density. We will treat these clusters separately in our discussion. We also measure the concentration index C for the above four clusters:

$$C = \log(R_{60}/R_{20}), \quad (1)$$

(BO84), where R_{20} and R_{60} are the radii which contain 20 and 60 per cent of the whole cluster populations, respectively. C is always larger than 0.35, and they are classified as either compact or intermediate clusters.

2.3 Field Galaxy Subtraction

The next ingredient that is needed for the accurate comparison between local and distant clusters is the foreground/background galaxy subtraction. We use the spectroscopic redshifts as the primary information of the cluster membership, where they are available. We define the cluster members as those whose peculiar velocities are within ± 3000 km s^{-1} from the cluster central velocity, and the galaxies outside of this redshift range are assumed to be field galaxies. This criteria is robust (Yee & Ellingson 1996). However, the depth of the spectroscopic redshifts is quite shallow (r=21.5), and also there are many galaxies for which spectroscopic redshifts are unavailable even brighter than this magnitude limit.

Therefore, we use a statistical method to determine cluster membership for the galaxies without spectroscopic information. The details of this method is given in Appendix A. Just a brief summary is given below. We take the sample of field galaxies from the edge of the CNOC clusters. From the distribution of these galaxies on the CM diagram, we know the probability that a given galaxy in a cluster with a given set of colour and magnitude is a field galaxy. Using this probability, we apply Monte-Carlo simulations to assign cluster membership statistically for each galaxy, and subtract the statistical non-members from the CM diagrams. The Monte-Carlo simulation is repeated 100 times per cluster and we average the realisations for the analyses presented in this paper, although the Poisson error is always larger than the error associated in the statistical field subtraction. Filled symbols in Fig. 1 show the resulting field corrected CM diagrams for a typical run.

2.4 Local Cluster Comparison

We use Coma as a representative rich local cluster for comparison with the CNOC clusters at higher redshifts. We take the high precision Coma photometric data from Terlevich et al. (2000). They imaged Coma in U and V bands with a spatial coverage of 3360 arcmin^2. We use a fixed diameter aperture of 25.3 arcsec both for the magnitudes and the color, which corresponds to a physical scale of 17 kpc. The measurement error is very small, and the typical error in $U-V$ colour is less than 0.035 magnitude. R_{30} for Coma is 22 arcmin or 0.9 Mpc (BO84; Merritt 1987). We fit the CM relation for galaxies within R_{30} and brighter than M_V>−20 using the Bi-weight method. The location of the red envelope is defined 0.073 magnitude redder than the fitted CM relation (red sequence) with the same slope of −0.12. This colour offset is obtained as a colour difference of the SSP models between $z_{\rm form}$=2 and 5.4 with solar metallicity, which is the same definition of the red envelopes for the CNOC clusters as used in § 3.1. The CM diagram of Coma within R_{30} is given in the bottom right panel of Fig. 6.

Note that we will not take into account the dynamical evolution of clusters in this paper. An estimate of this effect shows that it is unlikely to be important if we restrict attention to the region within R_{30}. According to the extended Press-Schechter (P-S) theory (Bower et al. 1991; Bond et al. 1991; Lacey & Cole 1993), a rich cluster comparable to

Coma had acquired ∼60 per cent of the present-day mass by z=0.33 (q_0=0.1). Judging from the X-ray luminosity, two of our sample clusters, A2390 and MS1358+62, will evolve into richer systems than Coma by the present-day. Although there is no such rich counterpart nearby to be directly compared, data on the dependence of the CMR with richness suggests that it would have even tighter CM ridge-line than that of Coma (Bower et al. 1992; López-Cruz 1996). If this is the case, the recent star formation would be more restricted and earlier truncation would be required for these clusters than that discussed in this paper. In addition, most of the galaxies within R_{30} at intermediate redshifts will locate in slightly smaller region than R_{30} at the present-day, because the cluster will acquire still ∼40 per cent of new galaxies between z=0.33 and z=0 for example. Therefore, the population within R_{30} at a z=0.33 cluster should be actually compared with those within R_{18} at z=0, where R_{18} is the radius which contains 18 per cent of the whole cluster population. However, the colour scatter within R_{30} of Coma is already so small that it hardly changes within this radius.

3 THE BUTCHER-OEMLER EFFECT

3.1 Blue Galaxy Fraction

From the field corrected CM diagrams (Fig. 1) we now calculate the blue galaxy fraction in each cluster. We follow the original BO definition of the blue galaxies, where only galaxies within R_{30} and those brighter than M_V=−20 in the rest frame are considered, and those bluer than $\Delta(B-V)$=−0.2 from the red sequence are defined as the 'blue' cluster members. We transform these BO's criteria of blue galaxies into the ones for the CNOC g and r bands in the observer's frame using the K-corrections given in Fukugita, Shimasaku & Ichikawa (1995). They based on Kennicutt's (1992) and Coleman, Wu & Weedman's (1980) spectral atlas. According to Fukugita et al. (1995), $\Delta(B-V)$=−0.2 roughly corresponds to Sab-type in the Hubble sequence of the present-day galaxies assuming the zero-point corresponds to E-type, and it can be transformed into $\Delta(g-r)$ at a given redshift as a colour difference between E and Sab types. The BO criteria $\Delta(B-V)$=−0.2 actually falls between Sab and Sbc types, and we make interpolation to get the exact $\Delta(g-r)$. This also corresponds to $\Delta(U-V)$=0.54 at the present-day, which is used as a BO criterion for our Coma data. The magnitude cut, M_V=−20, is also transformed into an apparent magnitude in r-band, $r_{\rm cut}$, for each cluster, assuming the E-type spectral energy distribution (SED) as in BO. The adopted $r_{\rm cut}$ and $\Delta(g-r)$ for each cluster are summarised in Table 1. They are also shown by the dot-dashed and the dotted lines in Fig. 1, respectively. However, the above magnitude cut is not correct for the blue galaxies. A blue galaxy with a given observed r magnitude is actually fainter in M_V than a red galaxy with the same r magnitude if the r-band in the observed frame corresponds to shorter wavelength than the rest frame V-band, as is actually the case for our CNOC clusters. Therefore, we apply colour dependent K-corrections using the numbers for various spectral types given in Fukugita et al. (1995). The BO magnitude cut in r-band thus determined is shown by the slanted dashed line in Fig. 1. The deviation from the constant $r_{\rm cut}$ (dot-dashed) is larger for blue $g-r$ colours and it also increases with redshifts. Therefore, the original BO definition of the magnitude cut tends to overestimate the fraction of blue galaxies by as much as 15 per cent as is shown later.

For each cluster, we define the location of a red sequence on the CM diagram as a zero-point from which we measure the colour difference. Since the CM slope is poorly determined with the CNOC photometry, we use a model prediction, assuming the CM slope is governed by metallicity variation. We adopted the metallicity sequence model in Kodama & Arimoto (1997). The model slope is calibrated to reproduce the Coma CM slope in $U-V$ and $V-K$ (Bower et al. 1992) at 15 Gyr. Since the CM slope depends on aperture within which we integrate colours, we adopt the 50 kpc aperture models to closely match the CNOC's large aperture (cf., Kodama et al. 1998). Using this fixed slope, the CM red sequence is fitted to the observed data so that the dispersion is minimised around the fitted line after rejecting the galaxies locating outside of one sigma for all the galaxies. The slopes and the zero-points at $r_{\rm cut}-1.5$ of the adopted CM red sequences are given in Table 1.

The 'red envelope' is also defined which we will use later in § 4. We assume that the 'red sequence' corresponds to $z_{\rm form}$=2, supposing it is the typical star formation epoch of cluster ellipticals (eg., Bower et al. 1992; Ellis et al. 1997; Stanford, Eisenhardt & Dickinson 1998; BKT98; Kodama et al. 1998; van Dokkum et al. 1998a; 1998b), and draw the red envelope parallel to the red sequence so that the envelope is redder than the sequence by the same amount of colour difference (in $g-r$) between a SSP model of $z_{\rm form}$=2 (T_G=12.3 Gyr) and that of $z_{\rm form}$=5.4 (T_G=15 Gyr). The colour difference ranges from 0.05-0.1 magnitude.

Following all these steps, we reproduce the definition of the blue galaxy fraction (f_B) used by BO84, with the addition of a colour dependent magnitude cut as discussed above. The blue fraction of each of the clusters is summarised in Table 1. Figure 2 shows f_B as a function of cluster redshift. Our results fit the original evolution line (solid line) suggested by BO84 remarkably well. The error bars in the plot indicate the pure Poisson errors. We have also estimated the error from the statistical field subtraction by a 100 Monte Carlo runs, but this is always much smaller than the Poisson error and is neglected. For comparison, values of f_B calculated without considering the colour dependent magnitude cut are also shown by crosses and the dotted error bars. Although the differences are smaller than the error bars, this systematic effect is typically 10-15 per cent for higher redshift clusters in a sense that the blue fraction is overestimated.

For A2390 and MS1621, we can cross-compare f_B with the earlier estimates by Abraham et al. (1996) and Morris et al. (1998), respectively. f_B=0.14±0.05 for A2390 and f_B∼0.2 for MS1621 at our R_{30} are both consistent with our estimate within the errors. It is notable, however, that one cluster, MS1512+36 at z=0.37, has anomalously high blue galaxy fraction compared to the BO84 line and the other CNOC clusters. The CM diagram of this cluster suggests that there may be a fourground group/cluster superimposed in the line of sight. There are ∼5 bright galaxies (r<19) with similar colour ($g-r$∼0.6) within R_{30} which are not subtracted in the statistical realisations. This clump appears to continue down to fainter magnitude and to form

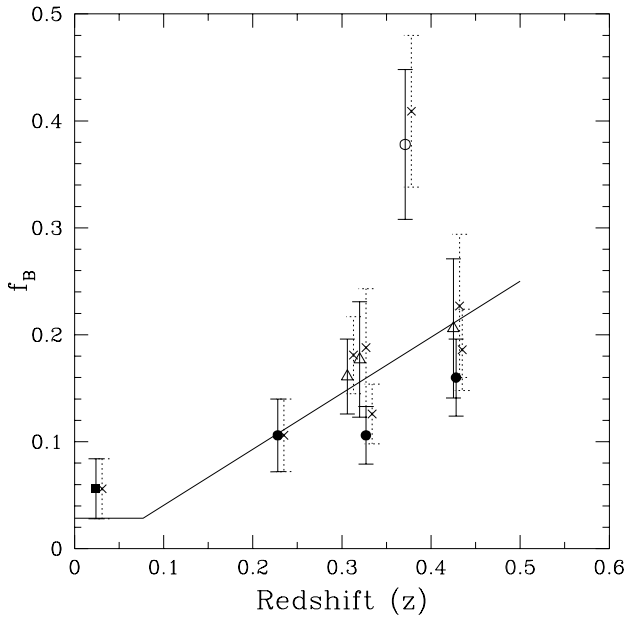

Figure 2. The blue galaxy fraction (f_B) in clusters as a function of redshift (see text for definition). The error bars indicate the Poisson errors. The solid line represents the original evolution line presented by BO84. Open triangles show the clusters for which we had to assume R_{30} due to the small spatial coverage. Coma cluster is also plotted by filled square. Crosses show the effect of neglecting the colour dependent K-corrections for the magnitude cut (see text for detail).

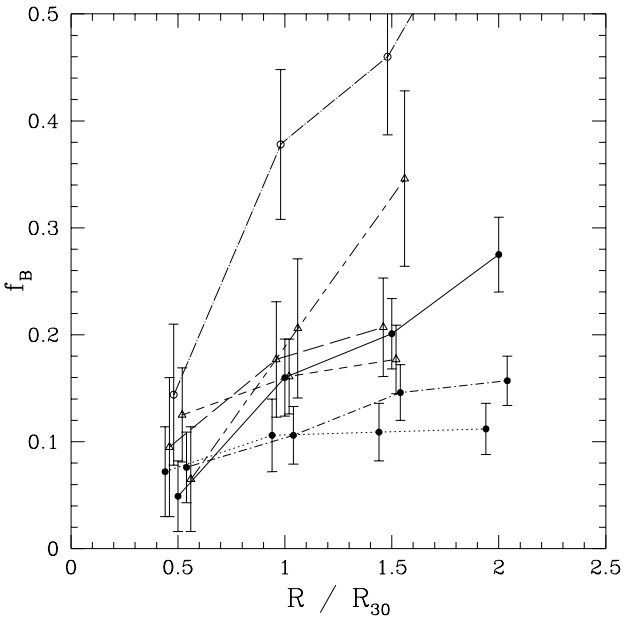

Figure 3. Dependence of the blue galaxy fraction on the radius (R) from the cluster centre within which f_B is defined. The radius is normalised using R_{30}. Seven lines show A2390 (dotted), MS1008−12 (short dashed), MS1224+20 (long dashed), MS1358+62 (short dash-dotted), MS1512+36 (long dash-dotted), MS0302+17 (long-short dashed), and MS1621+26 (solid), respectively. The points are slightly offset horizontally to avoid their overlapping.

another CM sequence. In fact, there are 5 more galaxies in the entire cluster field which have similar colour of $g-r\sim0.6$ within the very small spectroscopic redshift range of 0.163±0.002. At this redshift, the colour is consistent with passively evolving early-type galaxies (Kodama & Arimoto 1997), which leads us to suggest that the high value of the blue fraction of MS1512+36 is contaminated by the foreground group/cluster. For this reason we also exclude this cluster when we take the field sample from the edge of the observed area for the field correction, even though it has a relatively wide field of view.

3.2 Dependence on Radius

One of the interesting questions concerning the blue galaxies is their spatial distribution. If the galaxies are continuously falling in from the surrounding field, we should expect the blue galaxies to be located in the outskirts of the cluster. To test for this radial dependence, we create the CM diagrams for 0.5-2 R_{30}. If the radius exceeds the observed strip, we statistically sample galaxies at the same radii within the observed field.

Fig. 3 shows a general trend for f_B to increase with radius. This is to be expected, since it mainly reflects the density-morphology relation present in the intermediate redshift clusters (Dressler et al, 1997). This trend is consistent with the previous result shown by BO84, Abraham et al. (1996) and Morris et al. (1998). However, it illustrates how important it is that distant and local clusters are compared within equivalent radii.

3.3 Dependence on Magnitude

Another important issue is the magnitude dependence of the blue fraction. We investigate this by varying the magnitude cut above which the blue fraction is calculated. Fig. 4 shows how the blue fraction depends on magnitude. Only the two highest redshift clusters (MS1512+36 and MS1621+26) show a trend that f_B increases toward fainter magnitude. However, this may be caused simply by increasing photometric errors with magnitude. The remainder of the clusters show no significant trend: thus although examination of the colour-magnitude diagrams (Fig. 1) suggest that the blue galaxy population is predominantly faint, this reflects the increasing numbers of faint galaxies, rather than a systematic change in the blue fraction. To fully discuss the magnitude dependence of star formation histories, we need to consider the fading vectors of these galaxies.

4 FROM INTERMEDIATE REDSHIFT CLUSTERS TO THE COMA CLUSTER

In this section, we address the fate of the blue galaxies seen in the intermediate redshift clusters. In particular, we investigate whether they become incorporated into the tight CM relation seen in the present-day local clusters.

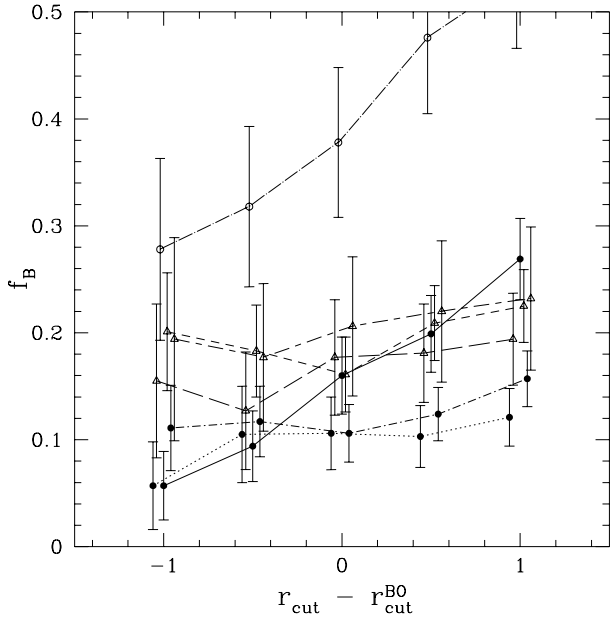

Figure 4. Dependence of the blue galaxy fraction on the magnitude cut ($r_{\rm cut}$). The magnitude cut is presented with respect to the one which corresponds to the BO's magnitude cut (M_V=−20). Seven lines show A2390 (dotted), MS1008−12 (short dashed), MS1224+20 (long dashed), MS1358+62 (short dash-dotted), MS1512+36 (long dash-dotted), MS0302+17 (long-short dashed), and MS1621+26 (solid), respectively. The points are slightly offset horizontally to avoid their overlapping.

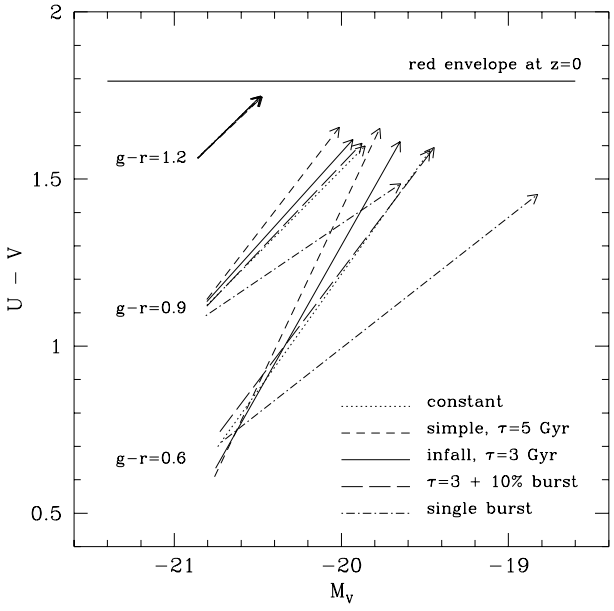

Figure 5. Fading/Reddening vectors from z=0.327 to z=0 on the rest frame $U-V$ and M_V diagram. Three sets of vectors are plotted for three galaxies with different colours at z=0.327; $(r, g-r)$=(21,0.6),(21,0.9), and $(21, 1.2)$. Five vectors correspond to different star formation histories we assume prior to the truncation epoch of the star formation; ie., (1) *Dotted line*: Constant star formation. (2) *Short dashed line*: Exponentially decaying star formation with an e-folding time of τ=5 Gyr (simple model). (3) *Solid line*: Infall model with τ=3 Gyr (see Appendix B for detail). (4) *Long dashed line*: The same as (3), but a 10 per cent burst is added just before the truncation. (5) *Dash-dotted line*: Single star burst just before the truncation. We assume that the star formation starts at $t_{\rm LB}$=15 Gyr (z=5.4) for all the models except (5) and terminates at the truncation epoch immediately. No residual star formation is considered. Horizontal solid line represents the red envelope at z=0. Metallicity in the models is fixed at solar value (Z=0.02).

BKT98 discussed this issue introducing the models where the star formation is truncated at the time of galaxy infall from the surrounding field to clusters. Estimating the distribution of the truncation epoch by the extended P-S theory, they explored the allowed star formation histories in rich clusters. In this paper we discuss this problem in further detail with taking into account the fading of the galaxies as well as reddening after the truncation of star formation. We use the stellar population synthesis code of Kodama & Arimoto (1997) as in BKT98. Instead of using the predicted galaxy infall rate at the first place, we start from the real galaxy distribution on the CM diagrams of intermediate redshift clusters, apply the star formation truncation model for the individual galaxies, and sketch the whole movement of cluster galaxies on the CM diagrams down to the present-day. We compare the final CM diagrams with that of Coma.

Initially, a difficulty with this approach *appears* to be that the photometric evolution of a galaxy after the end of its star formation, will depend on the star formation history we assume before the truncation. Fortunately, this is not the case: so long as a fraction of stars are old, the passive evolution phase is only weakly dependent on the previous history. Fig. 5 shows some examples of evolution vectors from z=0.327 to 0 for three galaxies with different colours ($g-r$=0.6, 0.9, and 1.2). For each galaxy, we plotted 5 different vectors which correspond to different star formation histories we assume as indicated in the figure and its caption. Star formation is truncated prior to z=0.327 for all the models, with the truncation time ($t_{\rm trunc}$) being chosen so that each model has the same $g-r$ colour at the moment of observation. Apart from the single burst model which gives the maximum fading and the bluest colour at the present-day, all the other models show similar evolution vectors on the CM diagram in spite of rather large variations in their star formation histories. This remains true even if a burst of star formation is included just before the truncation epoch. As a result, the evolution of the cluster members on the CM diagrams depends little on their prior star formation history.

In order to concentrate on the age of stellar populations, we have fixed the model metallicity at solar value (Z=0.02) in this paper as in BKT98. Since the metallicity of cluster early-type galaxies changes along the CM relation (Kodama et al. 1998; Terlevich et al. 1999; Kuntschner 2000), we corrected for the CM slope to the observed colours as follows;

$$(g-r)_{\rm corrected} = (g-r)_{\rm observed} - {\rm slope} \times (r - r_0) \qquad (2)$$

where r_0=$r_{\rm cut}$−1.5 which corresponds to M_V=−21.5 in the rest frame. Although this correction should eliminate the systematic metallicity effect as a function of luminosity, we neglect any age-metallicity conspiracy (Worthey, Trager

& Faber 1996; Trager 1997; Shioya & Bekki 1998): young galaxies are supposed to be more metal rich, hence the age and metallicity effect on galaxy colours may cancel out each other to some extent. We return to consider age variations along the CM relation in § 5.

Before applying the truncation model, we have to correct a small zero-point mismatch between the observed colours and the model by comparing between the colour of the red sequence at r_0 and the SSP model with solar metallicity and $z_{\rm form}$=2. We shifted the observed $g-r$ colours (already corrected for the CM slope) by 0.0-0.15 magnitude. Although it is probably partly due to the zero-point uncertainties in the model and the observation, it may also due to the metallicity mismatch since we fixed the model metallicity at solar metallicity.

Another problem is that there are a few galaxies which have been assigned cluster membership, even though they are redder than the CM sequence. These objects cause problems because they are difficult to model within our stellar population code. Some of these galaxies may be background objects which have not been removed by the statistical subtraction process. Alternatively, these red objects are likely to be scattered from the red sequence due to the relatively large photometric errors toward fainter magnitudes. Unlike galaxies scattered blueward of the sequence, the offset of these galaxies would remain large as we evolve the cluster forward in time. We have therefore adopted the scheme of initial correcting these red galaxies back onto the CMR sequence. A similar correction is not required for the blue galaxies since the differences decline as the stellar population ages. Moreover, it should be noted that this scatter is not large enough to affect the blue galaxy fraction (f_B) significantly — as can be seen by comparing the deviation of red and blue objects from the CM sequence in Fig. 1.

We are now in a position to simulate the photometric evolution of the cluster galaxy population. Fig. 6 illustrates the evolution of three sample clusters (A2390, MS1358+62, and MS1621+26) forward in time down to the present-day (from the left panel to the right). All the cluster members within R_{30} are plotted after the field subtraction. Here we use the infall model prescription to describe the star formation in a galaxy (see Appendix B). Star formation is truncated after a short burst, if any, on entering in the cluster environment (Appendix C). Adding the burst is motivated to explain the frequent appearence of strong Balmer absorption features in the integrated spectra of galaxies in the intermediate redshift clusters (Barger et al. 1994; Poggianti et al. 1999; BKT98; but see also Balogh et al. 1999). Although we have ambiguity for the star formation and the gas infall time scales and the burst strength here, the subsequent evolution is rather insensitive to those values unless the burst population dominates as already discussed in this section. We assign the star formation/gas infall time scale τ and the truncation time $t_{\rm trunc}$ for each galaxy to reproduce its colour in $g-r$ at cluster redshift as explained in Appendix D in detail. Our approach differs from that of Smail et al. (1998) who applied a similar kind of truncation model, under the assumption that star formation was terminated in *all* the cluster members at the same epoch. Instead, we allow $t_{\rm trunc}$ to vary from galaxy to galaxy reflecting the way the cluster is being built up continuously over time. With this parameterisation, we can later discuss the galaxy infall history which forms the clusters (§ 5). Once the τ and $t_{\rm trunc}$ is assigned for each cluster member, the model gives its colour and magnitude evolution in the rest frame $U-V$ and M_V. Figure 6 is an example of the Monte-Carlo simulations using $e_{\rm loss}$=0 and $e_{\rm burst}$=0.01 (Model b). The colour is presented with respect to the red envelope at z=0.

If we compare the initial CM diagrams (left end panels) of those intermediate redshift clusters with that of Coma cluster (bottom right panel) in the same coordinates, it is obvious that there are more blue galaxies in the distant clusters and the scatter around the CM red sequence is larger. However, if we trace the movement of those blue galaxies forward in time, we see that the galaxies become redder rapidly as time passes and all get redder than the BO criteria of blue galaxies (dotted line) only in a few Gyr at most after the cluster redshifts. As a result, the colour scatter of the CM relation is becomes small enough by the present-day, especially at the bright end ($M_V<-20$), to be consistent with the observed scatter in Coma. A more precise comparison is not justified by the photometric accuracy of the CNOC data and our consequent treatment of objects scattered redward of the initial CMR. If the galaxy harrassment accompanies during the galaxy infall and strip off some stars from the galaxy as numerical simulations suggest (Moore et al. 1996; Moore et al. 1999a), the blue galaxies could fade more and result in even smaller present-day colour scatter at the bright end. On the basis of this comparison, this effect is not required by the data, however.

Not only do the galaxies become redder, but they also get fainter after the truncation event. In fact, most of the blue galaxies which pass the BO criterion at the cluster redshifts fade rapidly and evolve to faint galaxies with $M_V>-20$ by the present-day. Therefore, the blue galaxies at intermediate redshifts are *not* the counter-parts of the bright early-type galaxies seen in present-day clusters including S0's. This is consistent with Kelson et al.'s (1999) and Poggianti et al.'s (1999) result derived from the spectroscopic signatures of star formation activity. It would appear that bright early-types should have completed their star formation well beyond z=0.4. This seems to indicate that the cosmic down-sizing hypothesis (Cowie et al., 1996; Cowie, Songaila & Barger 1999), where star formation propagate to smaller units as the Universe ages, may apply to cluster galaxies as well. It is interesting to extend this analysis toward higher redshift clusters in order to more strongly constrain the formation of massive cluster members.

Initially, this result seems at odds with our conclusion that the blue galaxy fraction did not depend on the magnitude cut that is chosen. However, consideration of the shape of the luminosity function explains the paradox. Because of the fading effect, the luminosity function of the blue galaxies should be offset by about 1 mag: thus — if galaxies of all masses shared the same formation history — we should have expected to see the blue galaxy fraction actually increasing at brighter magnitudes at cluster redshifts. We do not see this effect, which leads us to the down-sizing hypothesis.

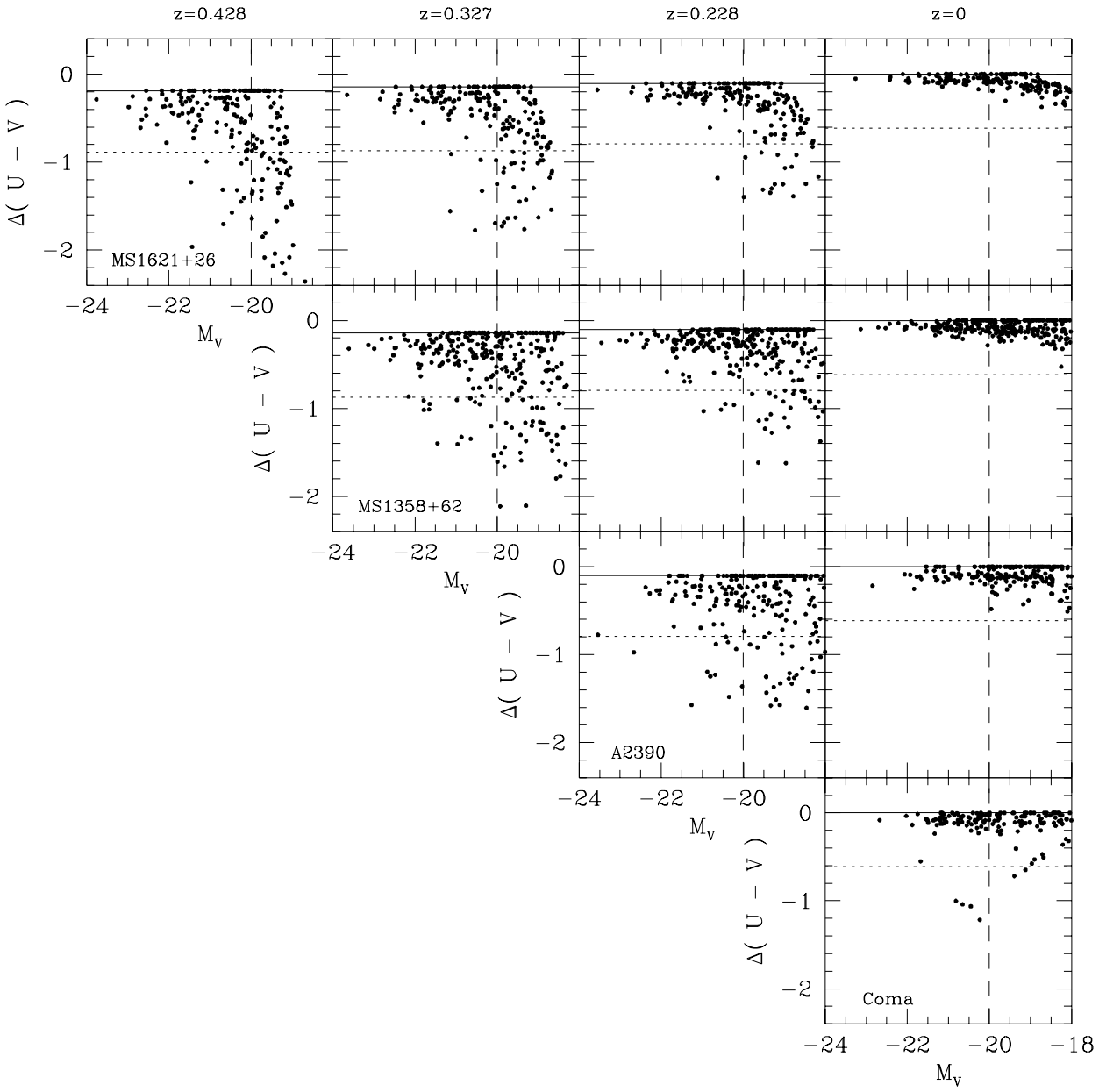

Figure 6. Evolution of the cluster galaxies within R_{30} forward in time on the CM diagrams. From the left panel to the right, redshift is decreasing as 0.428, 0.327, 0.228 and 0. Star formation is truncated after the infall of galaxy from the field following the continuous star formation which matches the Madau curve for the field. The truncation epoch ($t_{\rm trunc}$) is assigned for each galaxy to reproduce its $g-r$ colour at cluster redshift. This is an example of the Monte-Carlo simulations using $e_{\rm loss}$=0 and $e_{\rm burst}$=0.01 (Model b). See Appendices for the details of the modelling of star formation. Coma cluster is plotted in the bottom right panel to be compared with the z=0 models of the CNOC clusters. Colours are presented with respect to the red envelope (solid line) to eliminate the metallicity effect. The dotted line and the dashed line represent the BO criterion of the blue galaxies which corresponds to $\Delta(B-V)=-0.2$ and $M_V=-20$, respectively.

5 IMPLICATIONS FOR STAR FORMATION HISTORIES IN CLUSTER GALAXIES

In the previous section, we have modelled the photometric evolution of the cluster's galaxy populations in order to evolve the system forward in time. In this section, we look at the process from the other view-point: using the observed colour distribution to infer star formation and truncation histories in cluster environment from high redshifts down to the observed epoch.

We proceed as follows. As a starting point, we adopt a mix of galaxy star formation histories that are indicated by observations of distant field galaxies: the details are described in Appendix D. For each cluster, we are then able to infer a distribution of truncation times (following the scheme outlined in Appendix D) from the observed colour distribution. The whole process is treated in a Monte-Carlo sense, and many realisations are combined to produce the final distribution of truncation times. For example, a galaxy with only a small blueward deviation from the red CMR sequence might either be the result of a red (low star formation rate) field galaxy that arrived in the cluster recently, or of a blue (high star formation rate) field galaxy that arrived long before the observed epoch. Throughout, we will assume that the truncation of star formation is associated with the build up of the cluster from infalling field galaxies. Whereas we found that the direction of photometric evolution on the CM diagrams in the passive evolution phase has little model dependence, the time scale of the evolution immediately after the truncation epoch (and hence the colour distribution) does have considerable dependence on the way how the star formation is truncated (for example the burst strength and the level of residual star formation). It is therefore necessary to consider several different truncation schemes and to compare the cluster formation histories that they imply for the different clusters.

Figure 7 shows the resulting distribution of $t_{\rm trunc}$ for the galaxies brighter than $M_V=-19$ at $z=0$ for the three distant clusters, plus the nearby Coma cluster. The results of our Monte-Carlo simulations have been combined into three bins. Galaxies in which star formation has been recently truncated can be more accurately age-dated than older systems; thus age ranges of the bins increase to reflect the accuracy of the photometric data.

The two panels differ in the treatment of the truncation event. In model (a), we consider a violent event that might be expected to result from ram-pressure stripping (Abadi et al. 1999; Fujita & Nagashima 1999) or harrassment (Moore et al. 1996) of the galaxy as it arrives in the cluster. We assume that a half of the gas in the disk is consumed in a strong burst of star formation and that the remaining gas is lost from the system and no residual star formation is present afterwards. This model closely approximates the burst models used to explain the spectroscopic properties of E+A galaxies (eg., Couch & Sharples 1987; Poggianti et al. 1999). As can be seen, this model produces a skewed infall pattern in which the cluster accretion rate is always highest at the epoch of observations. This is not consistent with the smooth decline in the infall we had expected. If the infall occurs more erratically we would not expect to see the same excess in all the clusters. The fundamental problem with this model is that the blue galaxies evolve toward the red sequence so rapidly that the model struggles to produce the observed numbers of blue galaxies. We note, however, in the current model with $e_{\rm burst}$=0.5, the typical burst strength ($f_{\rm burst}$) at the time of truncation is only a few per cent in mass for those galaxies just arrived in the clusters. In order to avoid the peak in the accretion rate at the observed epoch, we could raise the burst strength so that the truncation epoch is pushed away into the past to get the same colour. However, this becomes effective only when we consider very strong burst at least 20 per cent in mass for *all* the galaxies. Under the current infall model scheme, an external gas supply is needed to produce such a strong burst, since the required amount of gas is not available for most of the galaxies.

In the second panel, model (b), we assume that there is no gass lost from the disk and that only 1 per cent of disk gas is converted into stars by a burst. In this case the dominant effect of the cluster is to suppress star formation by 'strangulation' — removing the halo of material that would otherwise have been slowly accreted by the galaxy (Larson, Tinsley & Caldwell 1980; Balogh et al. 2000). All the remaining gas is consumed exponentially with an e-folding time of 1 Gyr. This model produces a much more consistent picture of declining galaxy infall. For example, the predicted galaxy infall history for a z=0.33 cluster of mass 10^{15} $M_\odot$ is shown by the dashed lines. This has been estimated from the extended P-S theory using a threshold halo mass of $5{\cdot}10^{12}$ $M_\odot$ and $5{\cdot}10^{13}$ $M_\odot$ (for the right and left peaks respectively) at which the galaxy is counted as having made the transition from the field to cluster environment (Bower 1991; Kauffmann 1995). As can be seen the first of these models fits the data remarkably well. It is also notable that the infall history inferred from the Coma cluster matches smoothly onto that inferred from the higher redshift systems. This comparison gives us fundamental insight into the origin of the Butcher-Oemler effect (ie., the differences between low and high redshift clusters). Both the declining activity of field galaxies, and the declining rate at which galaxies are accreted from the 'field' environment play an important role in producing the consistency that we see in this diagram.

We can also use this approach to investigate the age trend along the CMR sequence. Since the blue galaxies fade and tend to enter into the faint end of the present-day CM relation, we should expect a systematic difference in stellar ages as a function of galaxy luminosity at the present-day. This effect could partly contribute for the CM slope. However, if the luminosity (B-band) weighted mean age of the galaxies ($t_{\rm lwm}$) measured at the present-day is plotted as a function of galaxy luminosity, the systematic trend is very weak; only $\sim$ 2 Gyr difference at most over 3-4 magnitude range of the present-day CM relation (Fig. 8). This plot has already been averaged over τ in the same way as in Fig. 7. The lack of magnitude dependence in luminosity weighted mean age reflects the fact that $t_{\rm lwm}$ gets old very rapidly once the star formation truncates and is rather insensitive to the recent star formation (BKT98): this explains why our finding can be consistent with the 'down-sizing' hypothesis considered in the previous section. What we see is that the scatter in age increases toward fainter magnitude, but this may be affected by the increasing photometric errors.

However, the systematic age difference is sensitive to the CM slope that we have subtracted to correct the metallicity effect. To see the maximum age variation that can be allowed

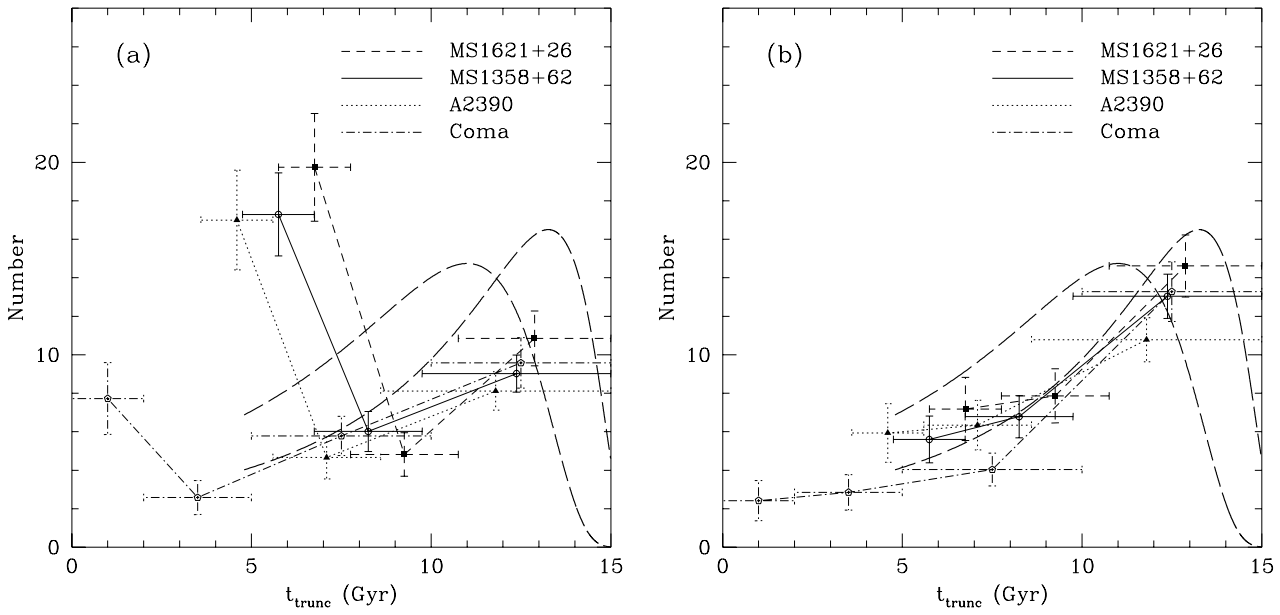

Figure 7. Distribution of the star formation truncation time ($t_{\rm trunc}$), which is equivalent to the galaxy infall time ($t_{\rm infall}$), for the galaxies with $M_V<-19$ at z=0. $t_{\rm trunc}$ is measured from the present-day rather than from the epoch at which the cluster is observed. The vertical axis gives the number of galaxies with this truncation time per Gyr and per 100 cluster galaxies. The bin sizes are set so that colour differences can be resolved within the photometric errors. Two cases are considered regarding the star formation at the galaxy infall. Left panel: In model (a), we assume that a half of the remaining gas in the disk is lost out of the system and the other half is turned into stars in a burst at the galaxy infall, and no residual star formation is present afterwards. Right panel: In model (b), we assume that no gass is lost from the disk and only a per cent of disk gas is converted into stars by a burst. All the remaining gas is consumed exponentially with an e-folding time of 1 Gyr. Thick dashed curves show the predicted galaxy infall history of a 10^{15} $M_\odot$ cluster at z=0.33 for a CDM-like power in an open universe (Ω_0=0.2, σ_8=0.8, Γ=0.1). The two curves in each plot are for threshold galaxy group mass of $5\cdot10^{12}$ $M_\odot$ (right) and $5\cdot10^{13}$ $M_\odot$ (left), respectively.

along the CM relation, we also do another set of simulation without correcting the CM slope at all. All the systematic effects are now attributed to age. Even in this extreme case, the age difference along the present-day CM relation is only $\lesssim$ 3 Gyr, or less than $\sim$20 per cent, and fails to reproduce the observed CM slope in Coma. This can contribute only a quarter of the aperture corrected present-day CM slope.

Finally, we use our approach to compare the global star formation history in the cluster environment with that of the universe as a whole. The global star formation history of the universe has received extensive attention since Madau et al. (1996) combined data on the local Hα luminosity (Gallego et al. 1995), the UV luminosity density from the CFRS survey (Lilly et al. 1995) and the Lyman Break galaxies (Steidel et al. 1995). This paper is an first attempt to show a similar plot for the galaxies in the *cluster* environment. Although we do not have direct observation at z>0.5, the data still probes star formation histories out to $z\sim1$ due to reasonably good sensitivity of the rest frame $U-V$ colour. For each cluster, we sum up individual star formation history over all the cluster members. In Fig 9 we show the integrated star formation histories for the galaxies in the rich cluster cores within R_{30} for the four clusters (Coma, A2390, MS1358+62, and MS1621+26). We rejected the brightest object, cD galaxy, in A2390 which would dominate the lowest redshift bin if present. The dotted and the dashed curves represent the Madau curve (Madau, Pozzetti, Dickinson 1998) for the field

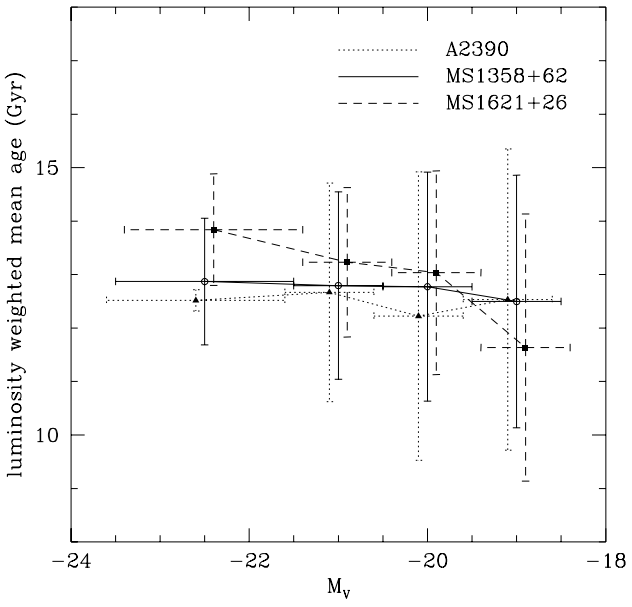

Figure 8. Luminosity weighted mean age at the present-day as a function of magnitude.

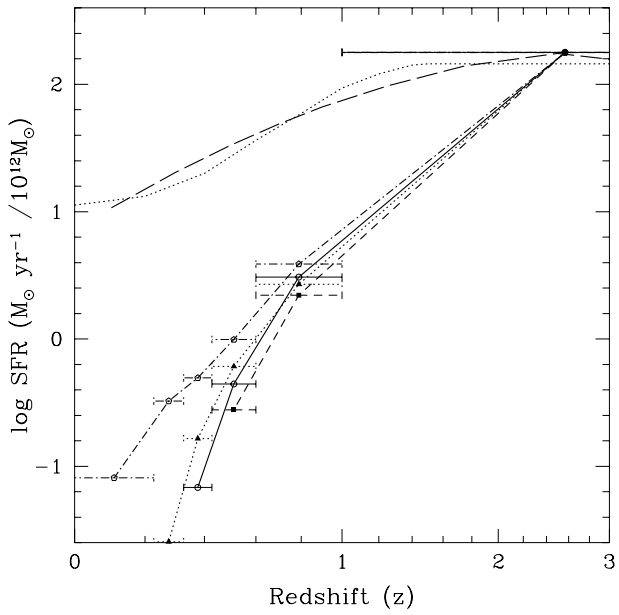

Figure 9. Madau plot for the galaxies in rich cluster cores (R_{30}). The star formation rate (SFR) is presented per galaxy mass of 10^{12} $M_\odot$. Four clusters are plotted individually by the curves with error bars; Coma (dot-dashed), A2390 (dotted), MS1358+62 (solid), and MS1621+26 (dashed). All the galaxies brighter than M_V=−19 at z=0 are included. The long dashed line above indicates the star formation history for the CNOC field galaxies. The dotted line above show the cosmic star formation history (field) taken from Madau et al. (1998).

environment, and the star formation history for the CNOC field galaxies, respectively. The curves are normalised per galaxy mass of 10^{12} $M_\odot$. We assumed the Madau curve is constant beyond z=1.5 in this normalisation, since otherwise the zero-point of the curve would be shifted upwards substantially due to the decline of the original curve beyond z=1.5. In the cluster cores, it is shown that the star formation at low redshifts is much more truncated than the field. At $z = 0.5$, the typical star formation rate per galaxy mass is more than a factor 10 smaller in the cluster cores, with galaxy formation skewed to higher redshifts. This is in qualitative agreement with Balogh et al. (1998) and Couch et al. (2000, in preparation) who show decline of the star formation rate from the field to the cluster environment at intermediate redshifts, measured by [OII] and Hα emission intensity, respectively. We should note however that the exact locus of cluster star formation history on this plot depends on the treatment of the truncation, especially on the amount of gas that is lost from the system upon infall to the clusters. The important next step is to map directly the star formation in the clusters and within individual galaxies to better understand the process of truncation. Hα star formation surveys (eg., Balogh & Morris 2000, submitted; Couch et al. 2000, in preparation) will be able to provide such information.

6 CONCLUSIONS

We have created the field corrected CM diagrams for the CNOC distant clusters (0.23<z<0.43), and discussed the blue galaxies therein defined in the same manner as in BO84. We make a comparison with the low redshift using data for the Coma cluster from Terlevich et al. (2000). The form for the redshift evolution of the blue galaxy fraction agrees well with the trend seen in BO84. In addition, the blue galaxy fraction is generally a strong increasing function of distance from the cluster centre, and depends only weakly on magnitude.

We have then applied these data-sets to build up a sequence of snap-shots of cluster evolution. We follow the evolution of the whole population of cluster galaxies in these CM diagrams accounting for the flow of galaxies across the diagram as they are accreted by the cluster.

- Firstly, we have shown that the blue galaxies are incorporated into the present-day tight CM relation as they fade and become redder rapidly after the truncation of their star formation, giving the possible link to the faint (>M_*+1) S0 galaxies in present-day clusters. The brighter S0 galaxies, however, must have truncated their star formation earlier than $z \sim 0.4$ in the context of the origin of cluster S0's followed by galaxy infall and truncation. Although the blue galaxies seen in the intermediate redshift clusters fade by ∼1 mag, these galaxies do not lead to a sizable age variation along the CM relation at the present-day.
- Secondly, we have used the distribution of galaxies in the colour space to infer the evolution of the rate at which galaxies have been accreted by the cluster. We interpret the observed distribution in colour by following the declining star formation rate in the field and statistically assigning a star formation truncation epoch. If star formation is truncated abruptly, we find that too many recent accretion events are required relative to the past rate. In order to be consistent with a smoothly declining accretion rate, such as suggested by the extended P-S theory, we need to allow for some level of residual star formation after galaxy infall. This suggests that the ram-pressure and/or mergers/harrassment cannot be so effective as to remove all the remaining gas from the system in a single orbital timescale. The BO effect is, thus shown to result from a combination of the three effects, namely, declining infall rate, declining field star formation rate, and the truncation of star formation.
- Finally, we have presented the global star formation history for the galaxies in rich cluster cores for the first time. It is shown that the star formation in cluster galaxies is much less than that in the field galaxies below z=1.

To resolve the star formation history in clusters at higher redshifts (z>1), we need a good homogeneous sample of clusters at higher redshifts (z>0.5-1.0). *Rosat* deep X-ray cluster survey (Rosati et al. 1998) and the coming new surveys by *Chandra* and *Newton* with high sensitivity cameras will provide ideal sample of high redshift clusters for this purpose.

The analysis presented in this paper, is limited by the accuracy of the the distant cluster photometry, as well as

by the number of clusters in our sample. A larger sample of clusters at each redshift would allow projection effects to be averaged over. Wider spatial coverage is also important to more accurately subtract field population and also to investigate the environmental effect beyond the cluster core out to the virial radius. This is essential if we are to improve our knowledge of the star formation truncation mechanism itself. At present, our approach is also compromised because we do not allow for the dynamical evolution of the cluster populations. Because of this, we cannot compare the properties of galaxies at different radii within the clusters. Recent rapid progress in the resolution N-body simulation of clusters (eg., Moore et al. 1999b; Balogh et al. 2000) will allow this aspect to be taken into account.

Acknowledgements

We are indebted to B. Abraham, H. Yee, and other CNOC group members for providing us their photometry catalogues and A. Terlevich for the Coma data which form the base of this work. We also thank I. Smail, M. Balogh, W. Couch and E. Bell for valuable discussions. T.K. thanks JSPS Research Fellowships for Young Scientists for financial support, and Univ. of Durham for kind hospitality during his stay in Durham. This project has made extensive use of Starlink computing facilities in Durham.

REFERENCES

Abadi, M. G., Moore, B., Bower, R. G., 1999, MNRAS, 308, 947
Abraham, R. G., et al., 1996, ApJ, 471, 69
Balogh, M. L., Shade, D., Morris, S. L., Yee, H. K. C., Carlberg, R. G., Ellingson, E., 1998, ApJ, 504, L75
Balogh, M. L., Morris, S. L., Yee, H. K. C., Carlberg, R. G., Ellingson, E., 1999, ApJ, 527, 54
Balogh, M. L., Navarro, J. F., Morris, S. L., 2000, submitted
Balogh, M. L., Morris, S. L., 2000, submitted
Barger, A. J., Aragón-Salamanca, A., Ellis, R. S., Couch, W. J., Smail, I., Sharples, R. M., 1996, MNRAS, 279, 1
Bond, J. R., Kaiser, N., Cole, S., Efstathiou, G., 1991, ApJ, 379, 44
Bower, R. G., 1991, MNRAS, 248, 332
Bower, R. G., Kodama, T., Terlevich, A., 1998, MNRAS, 299, 1193 (BKT98)
Bower, R. G., Lucey, J. R., Ellis, R. S., 1992, MNRAS, 254, 601
Brainerd, T. G., Smail, I., Mould, J. R., 1995, MNRAS, 275, 781
Butcher, H., Oemler, A., 1978, ApJ, 219, 18
Butcher, H., Oemler, A., 1984, ApJ, 285, 426 (BO84)
Coleman, C. D., Wu, C.-C., Weedman, D. W., 1980, ApJS, 43, 393
Couch, W. J., Newell, E. B., 1984, ApJS, 56, 143
Couch, W. J., Sharples, R. M., 1987, MNRAS, 229, 423
Couch, W. J., Ellis, R. S., Sharples, R. M., Smail, I., 1994, ApJ, 430, 121
Couch, W. J., Barger, A. J., Smail, I., Ellis, R. S., Sharples, R. M., 1998, ApJ, 497, 188
Cowie, L. L., Songaila, A., Hu., E. M., Cohen, J. G., 1996, AJ, 112, 839
Cowie, L. L., Songaila, A., Barger, A. J., 1999, AJ, 118, 603
Dressler, A., Gunn, J. E., 1992, ApJS, 78, 1
Dressler, A., Oemler, A., Butcher, H. R., Gunn, J. E., 1994, ApJ, 430, 107
Dressler, A., Oemler, A., Couch, W. J., Smail, I., Ellis, R. S., Barger, A., Butcher, H., Poggianti, B. M., Sharples, R. M., 1997, ApJ, 490, 577
Ebeling, H., Voges, W., Böhringer, H., Edge, A. C., Huchra, J. P., Briel, U. G., 1996, MNRAS, 281, 799
Ellis, R. S., Smail, I., Dressler, A., Couch, W. J., Oemler, A., Butcher, H., Sharples, R. M., 1997, ApJ, 483, 582
Fujita, Y., Nagashima, M., 1999, ApJ, 516, 619
Fukugita, M., Shimasaku, K., Ichikawa, T., 1995, PASP, 107, 945
Gallego, J., Zamorano, J., Aragón-Salamanca, A., Rego, M., 1995, ApJ, 455, L1
Gioia, I. M., Lupino, G. A., ApJS, 94, 583
Kauffmann, G., 1995, MNRAS, 274, 153
Kelson, D. D., Illingworth, G. D., van Dokkum, P. G., Franx, M., 1999, preprint, astro-ph/9906152
Kennicutt, R., 1992, ApJS, 79, 525
Kodama, T., Arimoto, N., 1997, A&A, 320, 41
Kodama, T., Arimoto, N., Barger, A. J., Aragón-Salamanca, A., 1998, A&A, 334, 99
Kuntschner, H., 2000, MNRAS, accepted (astro-ph/0001210)
Larson, R. B., Tinsley, B. M., Caldwell, C. N., 1980, ApJ, 237, 692
Lacey, C., Cole, S., 1993, MNRAS, 262, 627
Lilly, S. J., Tresse, L., Hammer, F., Crampton, D., Le Févre, O. 1995, ApJ, 455, 108
López-Cruz, O., 1996, PhD Thesis, Univ of Tronto
Lubin, L. M., 1996, AJ, 112, 23
Madau, P., Ferguson, H. C., Dickinson, M. E., Giavalisco, M., Steidel, C. C., Fruchter, A., 1996, MNRAS, 283, 1388
Madau, P., Pozzetti, L., Dickinson, M., 1998, ApJ, 498, 106
Merritt, D., 1987, ApJ, 313, 121
Moore, B., Katz, N., Lake, G., Dressler, A., Oemler, A., 1996, Nature, 379, 613
Moore, B., Lake, G., Quinn, T., Stadel, J., 1999a, MNRAS, 304, 465
Moore, B., Ghigna, S., Governato, F., Lake, G., Quinn, T., Stadel, J, Tozzi, P, 1999b, ApJ, 524, L19
Morris, S. L., Hutchings, J. B., Carlberg, R. G., Yee, H. K. C., Ellingson, E., Balogh, M. L., Abraham, R. G., Smecker-Hane, T. A., 1998, ApJ, 507, 84
Poggianti, B. M., Barbaro, G., 1996, A&A, 314, 379
Poggianti, B. M., et al., 1999, ApJ, 518, 576
Rakos, K. D., Schombert, J. M., 1995, ApJ, 439, 47
Rosati, P., Della Ceca, R., Norman, C., Giacconi, R., 1998, ApJ, 492, L21
Salpeter E. E., 1955, ApJ 121, 161
Schmidt, M., 1959, ApJ, 129, 243
Shioya, Y., Bekki, K., 1998, ApJ, 504, 42
Smail, I., Dressler, A., Couch, W. J., Ellis, R. S., Oemler, A. Jr, Butcher, H., Sharples, R. M., 1997, ApJS, 110, 213
Smail, I., Edge, A. C., Ellis, R. S., Blandford, R. D., 1998, 293, 124
Stanford, S. A., Eisenhardt, P. R. M., Dickinson, M., 1998, ApJ, 492, 461
Steidel, C. C., Pettini, M., Hamilton, D., AJ, 110, 2519
Trager, S. C., 1997, PhD Thesis, University of California, Santa Cruz
Terlevich,A.I., Kuntschner,H., Bower,R.G., Caldwell,N., Sharples,R. M., 1999, MNRAS, 310, 445
Terlevich, A. I., Bower, R. G., Caldwell, N., 2000, in preparation
Tinsley B. M., 1980, Fundamentals of Cosmic Physics, Vol.5, p.287
van der Marel, R. P., Magorrian, J., Carlberg, R. G., Yee, H. K. C., Ellingson, E., 1999, preprint (astro-ph/9910494)
van Dokkum, P. G., Franx, M., Illingworth, G. D., Kelson, D. D., Fisher, D., Fabricant, D., 1998a, ApJ, 500, 714
van Dokkum, P. G., Franx, M., Kelson, D. D., Illingworth, G. D., 1998b, ApJ, 504, L17

Worthey, G., Trager, S. C., Faber, S. M., 1996, in: Fresh Views of Elliptical Galaxies, eds. A. Buzzoni, A. Renzini, & A. Serrano (ASP Conf. Ser. Vol. 86)
Yee, H. K. C., Ellingson, E., 1996, Photometry Catalog for the CNOC clusters
Yee, H. K. C., Ellingson, E., Carlberg, R. G., 1996, ApJS, 102, 269

APPENDIX A1: STATISTICAL FIELD GALAXY SUBTRACTION

This appendix describes our method for subtracting the foreground/background populations from the cluster fields. The sample of field galaxies is taken from the edge of the cluster fields of three CNOC clusters with wide imaging fields; ie.,

$$\begin{array}{cc} 11 < \Delta\mathrm{RA} < 21 & \text{for A2390,} \\ 8 < \Delta\mathrm{DEC} < 11.5 & \text{for MS1358+62,} \\ \text{and } -12 < \Delta\mathrm{DEC} < -8 & \text{for MS1621+26,} \end{array}$$

where ΔRA and ΔDEC are the distances from the cluster centre in the unit of arcmin, and these correspond to $\gtrsim$3 Mpc which is comparable to or slightly smaller than the virial radius (Carlberg et al. 1996). After rejecting a few spectroscopically confirmed cluster members from this field area, the total number of the field galaxies is 871 down to r=23.5. Divided by the total area of 137.5 arcmin^2, it gives the field number density of 6.34 galaxies per arcmin^2. This can be compared to the deep field galaxy counts in Gunn's system (Brainerd et al. 1995) which has 90.1 arcmin^2 field of view and 7.01 galaxies per arcmin^2 with the same magnitude cut. Therefore our field sample can be regarded as a good representative of the field population. The CNOC field galaxies thus defined are plotted on the CM diagram in the bottom right panel of Fig.1.

We build the two dimensional distribution histogram of these field galaxies making the bins with a step of 0.3 in colour and 0.5 in magnitude. A similar histogram is also created for each cluster field within R_{30}. This obviously includes the field galaxies that are to be subtracted. The field histogram is normalised for each cluster to match the circular area within R_{30}. The number of spectroscopically confirmed non-members is then subtracted from these two histograms in each bin. Note the resulting number can be negative. We now count the number of galaxies in each bin (i,j) for the field ($N_{ij}^{\rm field}$) and the cluster field ($N_{ij}^{\rm cluster+field}$). The former can be larger than the latter for low density bins due to the low number statistics. If this happens, we re-distribute the excess number of field galaxies to the surrounding neighbouring bins (8, 5, or 3 bins depending on the location of the bin under concern) with equal weight until

$$N_{ij}^{\rm field} < N_{ij}^{\rm cluster+field} + 0.01 \tag{A1}$$

is satisfied in all bins. The last term, 0.01, is just for practical purpose so that the redistribution process can easily converge. We then define a probability, P, for each galaxy in the cluster field that it is a field galaxy:

$$P = \frac{N_{ij}^{\rm field}}{N_{ij}^{\rm cluster+field}}, \tag{A2}$$

where the numbers are taken from the bin that the galaxy belongs to. We now apply Monte Carlo simulations to statistically determine the field galaxies. We randomly pick out a membership-unknown galaxy from the entire CM diagram and refer its probability P to determine whether it should be regarded as a field galaxy. We repeat this process over the whole galaxies in the cluster field. We rerun the Monte Carlo simulation many times and average over the 100 realisations for each cluster.

APPENDIX A2: THE INFALL MODEL

We use the so-called infall model prescription for star formation in galaxies under the instantaneous recycling approximation (Tinsley 1980). We do not take into account the chemical evolution in the galaxy system in this paper, and the metallicity is fixed at solar value. To avoid confusion, this 'infall' means a 'gas infall' within a galaxy and has nothing to do with 'galaxy infall' from the field environment to the cluster which we also consider in this paper.

The galactic gas is supplied from a surrounding gas reservoir (halo) at the rate:

$$\xi_{\rm in}(t) = \frac{1}{\tau_{\rm in}} \exp(-\frac{t}{\tau_{\rm in}}). \tag{A3}$$

Total mass of the gas in the reservoir is normalised to unity. Zero-point of the time t is set to the look back time of 15 Gyr which corresponds to the redshift of 5.4 in our cosmology.

Schmidt law (Schmidt 1959) with a power unity is adopted where star formation rate is proportional to the gas density hence mass as

$$\psi(t) = \frac{1}{\tau_*} M_{\rm gas}(t), \tag{A4}$$

where $M_{\rm gas}$ indicates a mass of the infalled gas that is remained in gas state. $M_{\rm gas}(0)$ is set to zero. Note that this formulation gives an exponentially decaying star formation rate with an effective time scale $\tau_*^{\rm eff} = \tau_*/\alpha$ in the case of the simple models, where α is the so-called locked-up mass fraction defined by Tinsley (1980). The Salpeter mass function (Salpeter 1955), that we adopted in this paper with lower mass cut off 0.1 $M_\odot$ and the upper mass cut off 60 $M_\odot$, gives $\alpha = 0.72$.

For simplicity, we assume

$$\tau_*^{\rm eff} = \tau_{\rm in} \equiv \tau. \tag{A5}$$

This assumption leads to the simple analytic solutions for the star formation in a galaxy:

$$\psi(t) = \frac{1}{\alpha}\frac{t}{\tau^2} \exp(-\frac{t}{\tau}), \tag{A6}$$

which has a peak at $t = \tau$.

Gas mass and the stellar mass are given by:

$$M_{\rm gas}(t) = \frac{t}{\tau} \exp(-\frac{t}{\tau}) \tag{A7}$$

and

$$M_*(t) = 1 - (1 + \frac{t}{\tau}) \exp(-\frac{t}{\tau}), \tag{A8}$$

respectively.

Equations from (B1) to (B6), except (B3), are scaled for each galaxy to match its absolute magnitude.

APPENDIX A3: TRUNCATION AND STAR BURST

When a galaxy infalls from the field environment to the cluster ($t_{\rm infall}$), all the gas in the halo is assumed to be stripped off due to tidal stripping and the ram-pressure of the intracluster medium. This prevents further gas being supplied from the halo gas reservoir. A substantial fraction of the gas in a galaxy disk (ie., the material which has been accreted from the halo) may also be stripped away by the ram-pressure as the numerical simulations suggest (Abadi et al. 1999). Gas mass that is lost from the system is described by using the remaining gas mass and the gas loss efficiency parameter $e_{\rm loss}$ as

$$M_{\rm loss} = M_{\rm gas}(t_{\rm infall}) \times e_{\rm loss}. \quad \text{(A9)}$$

We allow a star burst to accompany the gas stripping process. Gas mass that is transformed into stars in the burst is described by a burst efficiency parameter $e_{\rm burst}$ and is given by

$$M_{\rm burst} = M_{\rm gas}(t_{\rm infall}) \times e_{\rm burst}. \quad \text{(A10)}$$

The burst strength is represented by the mass fraction of the burst population to the total stellar mass:

$$f_{\rm burst} = \frac{M_{\rm burst}}{M_*(t_{\rm infall}) + M_{\rm burst}}. \quad \text{(A11)}$$

After these processes, star formation in the galaxy is rapidly truncated. We assume that the star formation truncation time $t_{\rm trunc}$ is equal to the galaxy infall time $t_{\rm infall}$. After $t_{\rm trunc}$, the galaxy quickly consumes the remaining gas in the disk following the Schmidt low:

$$\psi(t) = \frac{1 - e_{\rm loss} - e_{\rm burst}}{\alpha \tau_{\rm trunc}} M_{\rm gas}(t_{\rm trunc}) \exp(-\frac{t - t_{\rm trunc}}{\tau_{\rm trunc}}) \quad \text{(A12)}$$

where $\tau_{\rm trunc}$ is a time scale for the truncation of star formation and is fixed to 1 Gyr.

The cases we consider in this paper are the following two:

Model	$e_{\rm loss}$	$e_{\rm burst}$
(a)	0.5	0.5
(b)	0.0	0.01

APPENDIX A4: ASSIGNING THE STAR FORMATION TIME SCALE AND THE TRUNCATION EPOCH

This section is devoted to explaining how we assign the star formation/gas infall time scale (τ) and the truncation epoch ($t_{\rm trunc}$) for each cluster galaxy.

Since we consider that the cluster galaxies infall from the field, the distribution of τ for the cluster galaxies is taken to be the same as for the field population. This is directly estimated from the colour distribution of the real field galaxies through our treatment of star formation described in Appendix B. Here we use 94 spectroscopically confirmed field galaxies between $0.3<z<0.35$ from the entire observed fields of the seven CNOC clusters. The estimated distribution of τ for the field galaxies can be expressed by a Gaussian:

$$\Phi(\tau) \propto \exp\{-\frac{1}{2}(\frac{\log\tau - \log\tau_0}{\sigma})^2\}, \quad \text{(A13)}$$

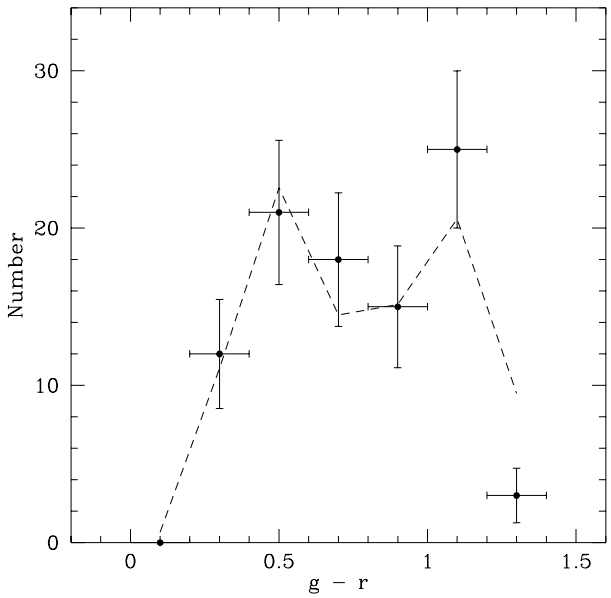

Figure A1. Distribution of $g-r$ colour for the spectroscopically confirmed field galaxies which locate between $0.3<z<0.35$. These galaxies are taken from all of our 7 CNOC cluster fields and the total number amounts to 94. Dashed line corresponds to the Gaussian distribution of τ for the field galaxies in equation (5).

where $\log\tau_0$=0.3, and σ=0.2. This distribution not only gives a reasonable match to the colour distribution of the CNOC field galaxies (Fig. A1), but also reproduces the so-called Madau curve (Madau et al. 1998); ie. the global star formation rate for field galaxies as a function of redshift at the same time (see the long dashed curve against the dotted curve in Fig. 9).

When the galaxies fall into clusters, star formation truncates with either gas loss and/or a star burst as described in Appendix C. Now, in order to reproduce a certain colour of a given cluster galaxy, various combination of τ and $t_{\rm trunc}$ is possible for a given set of $e_{\rm loss}$ and $e_{\rm burst}$, although τ should be larger than a certain minimum value $\tau_{\rm min}$ which corresponds to $t_{\rm trunc} = 0$.

For each possible combination of (τ,$t_{\rm trunc}$), the colour changing rate R at the cluster redshift is calculated:

$$R(\tau, t_{\rm trunc}) \equiv \left.\frac{d(g-r)}{dt}\right|_{z=z_{\rm cluster}}. \quad \text{(A14)}$$

Note the exception that the colour used is $U-V$ for Coma. The probability of assigning τ, $q(\tau)$, is inversely proportional to this rate since a galaxy with higher colour changing rate is rarer to find.

$$q(\tau) = \begin{cases} c/R(\tau, t_{\rm trunc}) & \tau \geq \tau_{\rm min} \\ 0 & \tau < \tau_{\rm min} \end{cases} \quad \text{(A15)}$$

where normalisation c is determined by

$$\int q(\tau) d\log\tau = 1. \quad \text{(A16)}$$

The distribution of τ is thus skewed towards larger values due to the minimum cut $\tau_{\rm min}$ and the $q(\tau)$ term. To

get the same distribution of τ in equation (D1) for the cluster galaxies, the probability of assigning a given τ should be corrected for these effects. The correction function $Q(\tau)$ is the sum of the individual $q(\tau)$ term over all the cluster members:

$$Q(\tau) = \Sigma q_i(\tau). \tag{A17}$$

Finally, we assign τ randomly for each cluster galaxy using the following distribution function $\Phi'(\tau)$:

$$\Phi'(\tau) = \Phi(\tau)/Q(\tau) \times q(\tau). \tag{A18}$$

The truncation time, $t_{\rm trunc}$, is then determined by requiring the galaxy to have its observed colour at the cluster look-back time.